Steel and Composite Structures, *Vol. 31, No. 5 (2019) 529-539*
DOI: https://doi.org/10.12989/scs.2019.31.5.529

Thermoelastic static and vibrational behaviors of nanocomposite thick cylinders reinforced with graphene

Rasool Moradi-Dastjerdi [a] and Kamran Behdinan[*]

Advanced Research Laboratory for Multifunctional Light Weight Structures (ARL-MLS), Department of Mechanical & Industrial Engineering, University of Toronto, Toronto, Canada

(*Received January 7, 2019, Revised April 2, 2019, Accepted April 13, 2019*)

Abstract. Current paper deals with thermoelastic static and free vibrational behaviors of axisymmetric thick cylinders reinforced with functionally graded (FG) randomly oriented graphene subjected to internal pressure and thermal gradient loads. The heat transfer and mechanical analyses of randomly oriented graphene-reinforced nanocomposite (GRNC) cylinders are facilitated by developing a weak form mesh-free method based on moving least squares (MLS) shape functions. Furthermore, in order to estimate the material properties of GRNC with temperature dependent components, a modified Halpin-Tsai model incorporated with two efficiency parameters is utilized. It is assumed that the distributions of graphene nano-sheets are uniform and FG along the radial direction of nanocomposite cylinders. By comparing with the exact result, the accuracy of the developed method is verified. Also, the convergence of the method is successfully confirmed. Then we investigated the effects of graphene distribution and volume fraction as well as thermo-mechanical boundary conditions on the temperature distribution, static response and natural frequency of the considered FG-GRNC thick cylinders. The results disclosed that graphene distribution has significant effects on the temperature and hoop stress distributions of FG-GRNC cylinders. However, the volume fraction of graphene has stronger effect on the natural frequencies of the considered thick cylinders than its distribution.

Keywords: natural frequency; thermal gradient load; temperature dependent graphene; nanocomposite thick cylinder; mesh-free method

1. Introduction

Two-dimensional graphene nano-sheet is one the most important allotropes of carbon which was first discovered by Novoselov *et al*. (2004). The thickness of graphene is one atom and due to its specific structures, graphene enjoys excellent strength and toughness as well as superior thermal conductivity, optical transparency and electrical conductivity (Balandin *et al*. 2008, Konatham and Striolo 2009, Kumar and Srivastava 2016, Li *et al*. 2018, Lin *et al*. 2017, Setoodeh and Badjian 2017, Shen *et al*. 2016). The mentioned properties of graphene make it an excellent candidate to produce advanced polymeric or metallic nanocomposites (Fan *et al*. 2018). In comparison with carbon nanotube (CNT) which is one of the most well-known nano-scale reinforcement candidate (Farahani *et al*. 2012), the interaction of graphene and matrix is higher also graphene is much cheaper (Kiani and Mirzaei 2018). Recently, the use of GRNCs in different engineering applications such as gas barrier (Cui *et al*. 2016, Yang *et al*. 2013), energy storage (Sun and Shi 2013) and Hydrogen sensing (Al-Mashat *et al*. 2010) has been reported (Shen *et al*. 2017b).

Thanks to the great properties of graphene nano-sheets, their nanoscale behavior (Alian *et al*. 2017, Ebrahimi and Barati 2018, Arani *et al*. 2013, Safaei and Fattahi 2017) and application as nanocomposite fillers have attracted the attentions of researches. Among the different mechanical analyses of GRNC structures, Rafiee *et al*. (2009) experimentally showed that using 0.1% weight fraction of graphene into a polymeric matrix caused 52% improvement in the buckling behavior of the resulted beams. Song *et al*. (2017, 2018) presented static and vibrational behaviors of multilayer GRNC plates using first order shear deformation theory (FSDT). They assumed graphene distribution in each layer to be uniformly distributed. However, using different values of graphene volume fractions for each layer, they considered FG multilayer GRNC plates. Wu *et al*. (2018) studied the instability of FG multilayer GRNC plates subjected to uniaxial pressures in thermal environment using differential quadrature method (DQM) and FSDT. Gholami and Ansari (2018a, b) utilized higher order plate theories to study the nonlinear natural frequencies and vibrational behavior of FG-GRNC plates subjected to harmonic mechanical loads. Nonlinear thermal stability, bending and postbuckling behaviors of FG multilayer GRNC beams resting on elastic foundations with temperature depended material properties were presented in (Kiani and Mirzaei 2018, Shen *et al*. 2017). Moreover, the nonlinear bending (Shen *et al*. 2017b), low-velocity impact (Fan *et al*. 2018), postbuckling (Yu *et al*. 2018) and forced vibration responses (Fan *et al*. 2019) of FG multilayer GRNC plates considering elastic foundations and thermal

*Corresponding author, Professor,
E-mail: behdinan@mie.utoronto.ca
[a] Ph.D., E-mail: moradi@mie.utoronto.ca

ISSN: 1229-9367 (Print), 1598-6233 (Online)

environments were also presented. For FG multilayer GRNC cylindrical panels, Shen *et al*. (2018) investigated nonlinear bending behavior using a two-step perturbation method and third order plate theory. Malekzadeh *et al*. (2018) used transformed DQM and FSDT to present the natural frequencies of FG multilayer GRNC irregular annular plates integrated with piezoelectric layers. Lei *et al*. (2018) developed a *kp*-Ritz mesh-free method based on FSDT to study the buckling behavior of FG-GRNC plates in thermal environments. Three-dimensional thermoelastic static behavior of FG-GRNC annular and elliptical plates with constant material properties at different temperatures were analytically reported in (Yang *et al*. 2017, 2018). Hosseini and Zhang (2018) utilized finite difference and Newmark methods to present a wave propagation and dynamic behavior of FG multilayer GRNC cylinders.

From the literature, the effect of thermal gradient load on the mechanical behaviors of GRNC axisymmetric thick cylinders have not been previously considered yet, however, this effect has been widely investigated in FGM structures (Damadam *et al*. 2018, Laoufi *et al*. 2016, Moheimani *et al*. 2018, Moheimani and Ahmadian 2012) and, CNT-reinforced nanocomposite structures using mesh-free methods (Moradi-Dastjerdi *et al*. 2018, Moradi-Dastjerdi and Payganeh 2017a, b, 2018, Safaei *et al*. 2018, 2019) or other methods (Alibeigloo and Liew 2013, Arani *et al*. 2011, Pourasghar *et al*. 2018, Pourasghar and Chen 2016, Sobhaniaragh *et al*. 2017). In this paper, axisymmetric thick cylinders reinforced with functionally graded randomly oriented graphene are considered. Thermoelastic static and free vibrational behaviors in the considered cylinders subjected to internal pressure and thermal gradient loads are presented. An axisymmetric mesh-free method is developed to study heat transfer and mechanical analyses of FG-GRNC cylinders. The temperature dependent material properties of GRNC are estimated using modified Halpin-Tsai model incorporated with two efficiency parameters. The effects of graphene distribution and volume fraction as well as thermo-mechanical boundary conditions on the temperature distribution, static response and natural frequency of FG-GRNC cylinders are presented.

2. Modeling of FG-GRNC thick cylinders

In order to study the thermoelastic behavior of uniformly distributed (UD) and FG-GRNC cylinders, first, temperature distributions in the cylinders are derived from steady state heat transfer equation. Then, the temperature and radial location dependent material properties are estimated using a modified Halpin-Tsai's approach. Finally, stress distribution and natural frequencies of GRNC thick cylinders with inner radius r_i, outer radius r_o and length L are calculated using the estimated material properties and a developed axisymmetric mesh-free method (see Fig. 1).

2.1 Estimation of material properties

The considered GRNC is assumed to be made of an isotropic polymeric matrix reinforced by randomly oriented graphene nano-sheets with length a_G, width b_G and

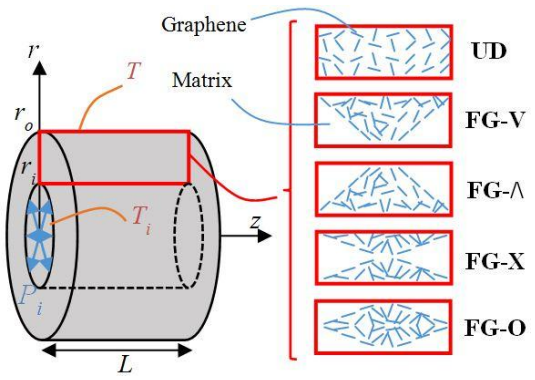

Fig. 1 Schematic figure of GRNC cylinder with different profiles for graphene distributions subjected to internal pressure

thickness h_G. The radial dependent thermal conductivity of FG-GRNC $k(r)$ are estimated by the following equation (Li *et al*. 2018, Shen *et al*. 2016)

$$k(r) = k^m \frac{3 + f_r(r)\left[2\beta_1(1-L_1) + \beta_3(1-L_3)\right]}{3 - f_r(r)\left[2\beta_1 L_1 + \beta_3 L_3\right]} \tag{1}$$

where

$$L_1 = \frac{p^2}{2\left(p^2-1\right)} - \frac{p}{2\left(p^2-1\right)^{3/2}}\cos^{-1} p\,,$$

$$L_3 = 1 - 2L_1\,, \qquad \beta_i = \frac{k_i - k^m}{k^m + L_i\left(k_i - k^m\right)}\,, \tag{2}$$

$$k_i = \frac{k^G}{1 + \gamma_k L_i k^G / k^m}\,, \qquad i = 1, 3\,,$$

$$\gamma_k = \left(1 + 2p\right) k^m R_k / h_G\,, \qquad p = a_G / h_G$$

where f_r is the volume fraction of graphene and superscripts G and m are used for graphene and matrix, respectively.

For the three-dimensional randomly oriented GRNC, the equation reported in (Craft and Christensen 1981) is employed to estimate thermal expansion coefficient α as below

$$\alpha = \frac{\left[E + 4\upsilon\left(1+\upsilon\right)K\right]\alpha_{11} + 4\left(1+\upsilon\right)K\alpha_{22}}{E + 4\left(1+\upsilon\right)^2 K} \tag{3}$$

where E, K and υ are effective Young's modulus, bulk modulus and Poisson's ratio of GRNC, respectively. The subscripts 11 and 22 show for longitudinal and transverse directions, respectively. The location and temperature dependent α_{11} (r, T) and α_{22} (r, T) in the nanocomposite reinforced with graphene nano-sheets are evaluated as follows (Shen *et al*. 2017b).

$$\alpha_{11} = \frac{f_r E_{11}^G \alpha_{11}^G + f_m E_m \alpha^m}{f_r E_{11}^G + f_m E_m} \tag{4}$$

$$\alpha_{22}(r,T)=(1+\upsilon^{G})f_r\alpha_{22}^{G}(T)+(1+\upsilon^{m})f_m\alpha^{m}(T)-\upsilon\alpha_{11}(T) \tag{5}$$

where $f_m = 1 - f_r$ is the volume fraction of polymeric matrix.

The effective Young's modulus of composite reinforced with randomly oriented fibers could be estimated using Halpin-Tsai's approach (Halpin and Kardos 1976). However, Shen *et al*. (2017b) modified this approach for the estimation of the mechanical properties of GRNC using two incorporating efficiency parameters (η_1 and η_2) to capture nano-scale effects (strain gradients, surface and intermolecular coupled stress between matrix and graphene nano-sheets) as follows (Halpin and Kardos 1976, Shen *et al*. 2017b)

$$E(r,T)=\frac{3}{8}\left[\eta_1\frac{1+2\left(a_G/h_G\right)\gamma_{11}^{G}f_r}{1-\gamma_{11}^{G}f_r}E^{m}\right]+\frac{5}{8}\left[\eta_2\frac{1+2\left(b_G/h_G\right)\gamma_{22}^{G}f_r}{1-\gamma_{22}^{G}f_r}E^{m}\right] \tag{6}$$

where

$$\gamma_{11}^{G}=\frac{E_{11}^{G}/E^{m}-1}{E_{11}^{G}/E^{m}+2a_G/h_G},\qquad \gamma_{22}^{G}=\frac{E_{22}^{G}/E^{m}-1}{E_{22}^{G}/E^{m}+2b_G/h_G} \tag{7}$$

where E_{ii}^{G} and E^{m} are Young's modulus of graphene nano-sheets and polymeric matrix, respectively. The employed efficiency parameters in Halpin-Tsai's model were extracted by Shen *et al*. (2017b) to match this model with MD results reported in (Lin *et al*. 2017) for the mechanical properties of GRNC for different temperatures and graphene volume fractions. Furthermore, the rule of mixture method is utilized to calculate the mass density ρ and effective Poisson's ratio υ of GRNC as below

$$\upsilon=f_r\upsilon^{G}+f_m\upsilon^{m},\qquad \rho=f_r\rho^{G}+f_m\rho^{m} \tag{8}$$

In this paper, linear distributions of graphene nano-sheets in the polymeric matrix are considered to find the best reinforcement behavior with the same volume fraction. For this purpose, a UD-GRNC cylinder as a comparator and four radial FG-GRNC cylinders (FG-V, FG-/\, FG-X and FG-O) are selected as depicted in Fig. 1. The described distributions can be formulated as follows (Moradi-Dastjerdi and Pourasghar 2016)

$$\text{UD:}\quad f_r(r)=\left(f_r^{\max}+f_r^{\min}\right)/2 \tag{9a}$$

$$\text{FG-V:}\quad f_r(r)=\Delta f_r\left(r-r_i\right)/h+f_r^{\min} \tag{9b}$$

$$\text{FG-/\:}\quad f_r(r)=\Delta f_r\left(r_o-r\right)/h+f_r^{\min} \tag{9c}$$

$$\text{FG-X:}\quad f_r(r)=2\Delta f_r\left|r-r_m\right|/h+f_r^{\min} \tag{9d}$$

$$\text{FG-O:}\quad f_r(r)=f_r^{\max}-2\Delta f_r\left|r-r_m\right|/h \tag{9e}$$

where $r_m = (r_i + r_o)/2$, r is radial location and Δf_r shows the difference between the minimum $f_r^{\min}$ and maximum $f_r^{\max}$ values of graphene volume fractions inside polymeric matrix.

2.2 Governing equations

We solved steady state heat transfer equation for FG-GRNC axisymmetric thick cylinders to obtain the temperature distribution $T(r, z)$ of the cylinders. This equation is given as (Alibeigloo and Liew 2013)

$$k(r)\frac{\partial^2T(r,z)}{\partial r^2}+\frac{\partial k(r)}{\partial r}\frac{\partial T(r,z)}{\partial r}+\frac{k(r)}{r}\frac{\partial T(r,z)}{\partial r}+k(r)\frac{\partial^2T(r,z)}{\partial z^2}=0 \tag{10}$$

where z is axial direction in the considered cylinders.

The constitutive law for isotropic and elastic FG-GRNC axisymmetric cylinders is expressed as

$$\boldsymbol{\sigma}=\mathbf{D}\boldsymbol{\varepsilon} \tag{11}$$

where stress vector $\boldsymbol{\sigma}$, mechanical strain vector $\boldsymbol{\varepsilon}$ and matrix $\mathbf{D}$ are defined as

$$\boldsymbol{\sigma}=\begin{bmatrix}\sigma_r & \sigma_\theta & \sigma_z & \sigma_{rz}\end{bmatrix}^{T},\quad \boldsymbol{\varepsilon}=\begin{bmatrix}\varepsilon_r & \varepsilon_\theta & \varepsilon_z & \varepsilon_{rz}\end{bmatrix}^{T},\quad \mathbf{D}=\frac{E}{(1+\nu)(1-2\nu)}\begin{bmatrix}1-\nu & \nu & \nu & 0\\ \nu & 1-\nu & \nu & 0\\ \nu & \nu & 1-\nu & 0\\ 0 & 0 & 0 & (1-2\nu)/2\end{bmatrix} \tag{12}$$

where θ is circumferential direction. In thermoelastic problems, both mechanical and thermal gradient loads can deform structures. Therefore, total strain in FG-GRNC axisymmetric cylinders subjected to thermo-mechanical loads includes mechanical and thermal strains. The relation between the vectors of mechanical strain $\boldsymbol{\varepsilon}$, thermal strain $\boldsymbol{\varepsilon}_T$ and total strain $\mathbf{e}$ is defined as

$$\mathbf{e}=\boldsymbol{\varepsilon}+\boldsymbol{\varepsilon}_T \tag{13}$$

where

$$e_r=\partial U_r/\partial r,\ e_\theta=U_r/r,\ e_z=\partial U_z/\partial z,\quad e_{rz}=\left(\partial U_r/\partial z\right)+\left(\partial U_z/\partial r\right) \tag{14}$$

$$\boldsymbol{\varepsilon}_T=\left[\alpha.\Delta T,\alpha.\Delta T,\alpha.\Delta T,0\right]^{T} \tag{15}$$

in which U_r and U_z are structural radial and axial displacements, respectively. $\Delta T = T - T_0$ is the difference between cylinder temperature T and T_0 = 300K (stress free or room temperature).

The weak form of motion equation for the dynamic behavior of FG-GRNC axisymmetric cylinders in the

absence of body forces is defined as (Moradi-Dastjerdi *et al*. 2017)

$$\int_{\Omega} \boldsymbol{\sigma}.\delta(\boldsymbol{\varepsilon})dv - \int_{\Gamma} \mathbf{F}.\delta\mathbf{u}ds = -\int_{\Omega} \rho(r)\,\ddot{\mathbf{u}}.\delta\mathbf{u}dv \tag{16}$$

where $\mathbf{u}$, $\ddot{\mathbf{u}}$ and $\mathbf{F}$ are the vectors of displacement, acceleration and surface traction, respectively.

3. Discretization with the mesh-free method

This section presents the development of a weak form mesh-free method based on MLS shape function to study thermoelastic behavior of FG-GRNC axisymmetric cylinders. Using MLS shape functions $\boldsymbol{\Phi}$, displacement vector $\mathbf{u}$ is approximated as follows (Safari *et al*. 2018)

$$\mathbf{u} = [u_r, u_z]^T = \boldsymbol{\Phi}\hat{\mathbf{u}} \tag{17}$$

where virtual nodal values vector $\hat{\mathbf{u}}$ and matrix $\boldsymbol{\Phi}$ are determined by

$$\hat{\boldsymbol{u}} = [(\hat{u}_r)_1, (\hat{u}_z)_1, \ldots\ldots\ldots (\hat{u}_r)_N, (\hat{u}_z)_N]^T \tag{18}$$

$$\boldsymbol{\Phi} = \begin{bmatrix} \Phi_1 & 0 & \Phi_2 & 0 & . & . & . & . & \Phi_N & 0 \\ 0 & \Phi_1 & 0 & \Phi_2 & . & . & . & . & 0 & \Phi_N \end{bmatrix} \tag{19}$$

in which Φ_i is the value of shape function at node i and N is the number of nodes inside the support domain of each Gauss point in background cells. Using Eqs. (13) and (17), strain vector can be expressed in terms of virtual nodal values

$$\mathbf{e} = \mathbf{B}\hat{\mathbf{u}} \tag{20}$$

where

$$\mathbf{B} = \begin{bmatrix} \frac{\partial\Phi_1}{\partial r} & 0 & \frac{\partial\Phi_2}{\partial r} & 0 & . & .. & . & . & \frac{\partial\Phi_N}{\partial r} & 0 \\ \frac{\Phi_1}{r} & 0 & \frac{\Phi_2}{r} & 0 & . & .. & . & . & \frac{\Phi_N}{r} & 0 \\ 0 & \frac{\partial\Phi_1}{\partial z} & 0 & \frac{\partial\Phi_2}{\partial z} & . & .. & . & . & 0 & \frac{\partial\Phi_N}{\partial z} \\ \frac{\partial\Phi_1}{\partial z} & \frac{\partial\Phi_1}{\partial r} & \frac{\partial\Phi_2}{\partial z} & \frac{\partial\Phi_2}{\partial r} & . & .. & . & . & \frac{\partial\Phi_N}{\partial z} & \frac{\partial\Phi_N}{\partial r} \end{bmatrix} \tag{21}$$

Substitution of Eqs. (11), (17) and (20) in Eq. (16) gives

$$\boldsymbol{M}\ddot{\hat{\boldsymbol{u}}} + \boldsymbol{k}\hat{\boldsymbol{u}} = \boldsymbol{f} + \boldsymbol{f}_T \tag{22}$$

in which mass matrix $\mathbf{M}$, stiffness matrix $\mathbf{k}$, mechanical force vector $\mathbf{f}$ and resulted thermal load vector $\mathbf{f}_T$ are presented as follows

$$\begin{aligned} &\mathbf{M} = \int_{\Omega} \rho\boldsymbol{\Phi}^T\boldsymbol{\Phi}dv, \qquad \mathbf{f} = \int_{\Gamma} \boldsymbol{\Phi}^T\mathbf{F}ds, \\ &\mathbf{k} = \int_{\Omega} \mathbf{B}^T\mathbf{D}\mathbf{B}dv, \qquad \mathbf{f}_T = \int_{\Omega} \mathbf{B}^T\mathbf{D}\boldsymbol{\varepsilon}_T dv \end{aligned} \tag{23}$$

It is worth noting that the eliminating of mass matrix or force vectors leads to governing equation for the static or free vibration analysis of considered FG-GRNC cylinders, respectively.

Moreover, the same mesh-free formulation is developed for axisymmetric steady state heat transfer equation as discretized in the following equation (Moradi-Dastjerdi *et al*. 2018, Moradi-Dastjerdi and Payganeh 2018)

$$\mathbf{k}_T \times \mathbf{T} = \mathbf{q} \tag{24}$$

in which thermal stiffness matrix $\mathbf{k}_T$, temperature vector $\mathbf{T}$ and flux vector $\mathbf{q}$ are determined as

$$\begin{aligned} &\mathbf{k}_T = \int_{\Omega} \mathbf{B}_T^T\mathbf{D}_T\mathbf{B}_T dv, \\ &\mathbf{T} = \begin{bmatrix} T_1 & T_2 & .... & T_N \end{bmatrix}^T, \qquad \mathbf{q} = \int_{\Gamma} \boldsymbol{\Phi}_T^T\mathbf{Q}ds \end{aligned} \tag{25}$$

where

$$\boldsymbol{\Phi}_T = \begin{bmatrix} \Phi_1 & \Phi_2 & .... & \Phi_N \end{bmatrix}^T,$$

$$\mathbf{B}_T = \begin{bmatrix} \frac{\partial\Phi_1}{\partial r} & \frac{\partial\Phi_2}{\partial r} & ... & \frac{\partial\Phi_N}{\partial r} \\ \frac{\partial\Phi_1}{\partial z} & \frac{\partial\Phi_2}{\partial z} & ... & \frac{\partial\Phi_N}{\partial z} \end{bmatrix}, \qquad \mathbf{D}_T = \begin{bmatrix} k & 0 \\ 0 & k \end{bmatrix} \tag{26}$$

4. Results and discussions

In this section, first the accuracy and convergence of the developed mesh-free method for thermoelastic problems have been verified. Then temperature, stress and displacement distributions as well as natural frequencies in GRNC thick cylinders subjected to mechanical and thermal gradient loads are evaluated. Temperature dependent nanocomposites are assumed to be made of PMMA as a polymeric matrix which is functional graded reinforced with graphene sheets as nanofillers. The length, width and thickness of graphene are a_G = 14.76, b_G = 14.77 and h_G = 0.188 nm, respectively (Lin *et al*. 2017). In the following simulations of GRNC, the temperature dependent thermal expansion coefficient and elasticity modulus of PMMA and graphene have been considered as given below (Shen *et al*. 2017a)

$$\begin{aligned} &E^m = (3.52 - 0.0034T)GPa, \\ &\alpha^m = 45(1 + 0.0005\Delta T)\times 10^{-6}/K \end{aligned} \tag{27}$$

$$\begin{aligned} &E_{11}^G = (2.16637 - 0.00193T + 2.93701\times 10^{-6}T^2 \\ &-1.51775\times 10^{-9}T^3)\ \text{TPa} \\ &E_{22}^G = (2.16868 - 0.00193T + 2.85954\times 10^{-6}T^2 \\ &-1.45145\times 10^{-9}T^3)\ \text{TPa} \\ &\alpha_{11}^G = (-3.83788 - 0.01416T - 1.63355\times 10^{-5}T^2 \\ &+6.33589\times 10^{-9}T^3)\times 10^{-6}/\text{K} \\ &\alpha_{22}^G = (-3.73997 - 0.01296T - 1.35033\times 10^{-5}T^2 \\ &+4.60392\times 10^{-9}T^3)\times 10^{-6}/\text{K} \end{aligned} \tag{28}$$

where T is the temperature (K) of GRNC cylinder. The other material properties of were assumed as: υ^m = 0.34, υ^G

Table 1 The utilized graphene efficiency parameters for different f_r and T (Shen, Xiang, *et al*. 2017)

	T = 300 K					T = 400 K					T = 500 K				
f_r	**0.03**	**0.05**	**0.07**	**0.09**	**0.11**	**0.03**	**0.05**	**0.07**	**0.09**	**0.11**	**0.03**	**0.05**	**0.07**	**0.09**	**0.11**
η_1	2.929	3.068	3.013	2.647	2.311	2.977	3.128	3.060	2.701	2.405	3.388	3.544	3.462	3.058	2.736
η_2	2.855	2.962	2.966	2.609	2.260	2.896	3.023	3.027	2.603	2.337	3.382	3.414	3.339	2.936	2.665

= 0.177, ρ^m = 1150, ρ^G = 4118 Kg/m^3, k^m = 0.247 W/mK (Shen *et al*. 2017a), k^G = 5000 W/mK (Balandin *et al*. 2008) and $R_k = 3\times10^{-9}$ K.m^2/W (Konatham and Striolo 2009).

The values of efficiency parameters (η_1 and η_2) are presented in Table 1 for different temperatures and graphene volume fraction (Shen *et al*. 2017b). It should be mentioned that a two-dimensional spline interpolation function is utilized to create a smooth variation in η_1 and η_2 with respect to graphene volume fraction and temperature.

Moreover, following non-dimensional parameters were utilized for displacement, stress and natural frequency (Moradi-Dastjerdi and Payganeh 2017a, 2018)

$$\bar{U} = \frac{U}{r_o\,\alpha^m T_0}, \bar{\sigma} = \frac{\sigma}{E^m\,\alpha^m T_0}, \Omega = \omega r_o\sqrt{\rho^m/G^m} \tag{29}$$

where ω is axisymmetric frequency of cylinder. E^m, α^m and G^m were evaluated at room temperature (T_0 = 300 K).

4.1 Validation of models

In this section, we verify the accuracy of the developed mesh-free method results by comparing with exact results. Therefore, the exact solutions of steady-state heat transfer and stress distributions for isotropic thick cylinders subjected to thermal gradient loads reported by Hetnarski and Eslami (2009) have been considered. Their reported equations are provided in Appendix.

Fig. 2 show temperature, hoop stress and radial stress distributions for two different thermal gradient loads of T_i = 300, T_o = 500 K and T_i = 500, T_o = 300 K at two different radius ratios of r_i/r_o = 0.5 and 0.75. The results clearly reveal that the developed method enjoys a very good accuracy in predicting the thermoelastic behavior of thick cylinders.

In order to examine the convergence of developed mesh-free method, the first axisymmetric natural frequency of an O-type FG-GRNC cylinder are calculated for different node arrangements along the radial and axial directions ($n\times n$). In the considered O-type GRNC cylinder, we assumed that the two ends of the cylinder are fixed (U_r and U_z = 0), r_i/r_o = 0.5, L/r_o = 1, T_i = 300 K, T_o = 500 K, $f_r^{\min}$ = 0.03 and $f_r^{\max}$ = 0.11. Fig. 3 shows that the developed mesh-free method is rapidly converged and after 25×25 node arrangement, there is a negligible variance in the predicted frequency. Moreover, it is observed that the error of predicted frequency with 5×5 node arrangement is less than 2 percent.

4.2 Steady state heat transfer in FG-GRNC cylinder

The effects of profile distribution and volume fraction of graphene upon the steady state heat transfer response of UD and FG-GRNC cylinders are shown in Fig. 4. Fig. 4(a) shows that, in comparison with other types of graphene distributions, using $\wedge$ and V types result in the corresponding cylinders to have higher temperature when T_i = 2 T_o and T_o = 2 T_i, respectively. Fig. 4(b) discloses that the decrease of graphene volume leads to more linear temperature distribution in FG-GRNC cylinders. According to Figs. 4, it can be concluded that by enhancing the overall thermal conductivity of nanocomposite, the use of graphene in different distribution profiles leads to considerable changes in the steady state heat transfer responses of FG-GRNC cylinders.

4.3 Static response of FG-GRNC cylinder

The effect of graphene distribution on the static responses of FG and UD-GRNC thick cylinders subjected

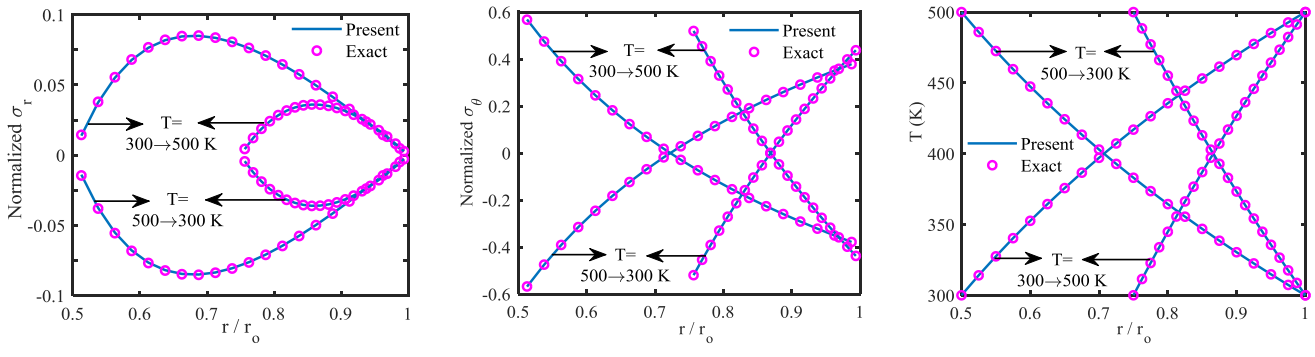

Fig. 2 Comparison of exact (Hetnarski and Eslami 2009) and mesh-free distributions of (a) normalized hoop stress; (b) normalized radial stress; (c) temperature along the radius of isotropic cylinders

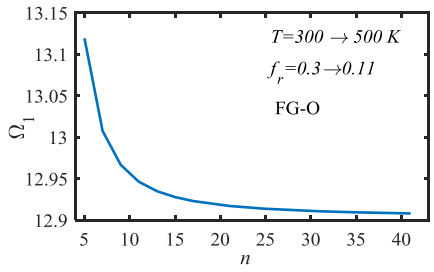

Fig. 3 Convergence of the first normalized natural frequency for clamped-clamped O-GRNC cylinder with r_i/r_o = 0.5 and L/r_o = 1

to thermal gradient loads is presented in Fig. 5. In these simulations, long cylinders with T_i = 300 K, T_o = 400 K, r_i/r_o = 0.75, f_r^{min} = 0.03 and f_r^{max} = 0.11 are considered. The results disclose that the profile of graphene distribution has a significant effect not only on the stress distributions but also on the radial deflection of the cylinders. Fig. 5(a) shows the values of radial stresses at internal and external radii are equal to mechanical pressures at these locations which are zero. However, the distribution of graphene governs the location and value of maximum radial stress. X and O-GRNC cylinders are exposed to the highest and lowest values of radial stress, respectively. Moreover, the maximum values of radial stresses in /\-type cylinder is observed at the inner half of cylinder thickness, but in V-type cylinders, it is happened at its outer half. Fig. 5(b) shows that O-type cylinder has the minimum value and minimum gradient of hoop stress along the cylinder thickness. However, the highest values of hoop stress are observed in X-GRNC cylinder. According to Fig. 5(c), V and /\-GRNC cylinders under thermal gradient loads have the highest and lowest values of radial deflections, respectively.

Fig. 6 illustrate the effect of graphene volume fraction on the static response of O-GRNC cylinders subjected to thermal gradient loads (T_i = 300 K, T_o = 400 K) and internal pressure (P_i = 10 MPa). The increase of graphene volume fraction increases all values of stresses although it decreases the radial deflection values. Furthermore, the application of internal pressure for cylinders under thermal gradient loads results in an intensification in radial and hoop stress values only at the inner half of cylinder thickness. Fig. 6(c) shows that internal pressure leads to a significant increase in radial deflections, especially in lower values of f_r^{max}.

Radial and hoop stress distributions along the radius of V and /\-GRNC thick cylinders with T_i = 300 K, f_r^{min} = 0.03, f_r^{max} = 0.11, and r_i/r_o = 0.75 for different outer temperatures T_o are shown in Figs. 7(a) and (b), respectively. Furthermore, Fig. 8 show similar results for cylinders with r_i/r_o =

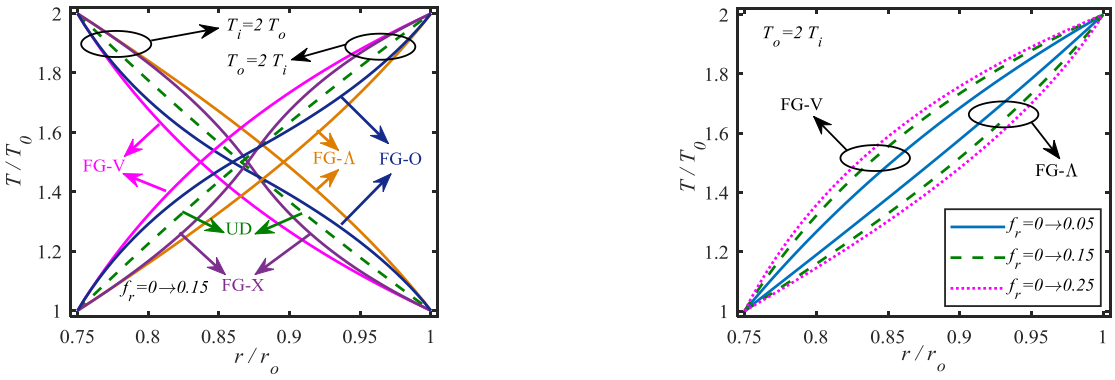

Fig. 4 The effects of graphene (a) profile distribution; and (b) volume fraction on the steady state heat transfer response of FG-GRNC cylinders

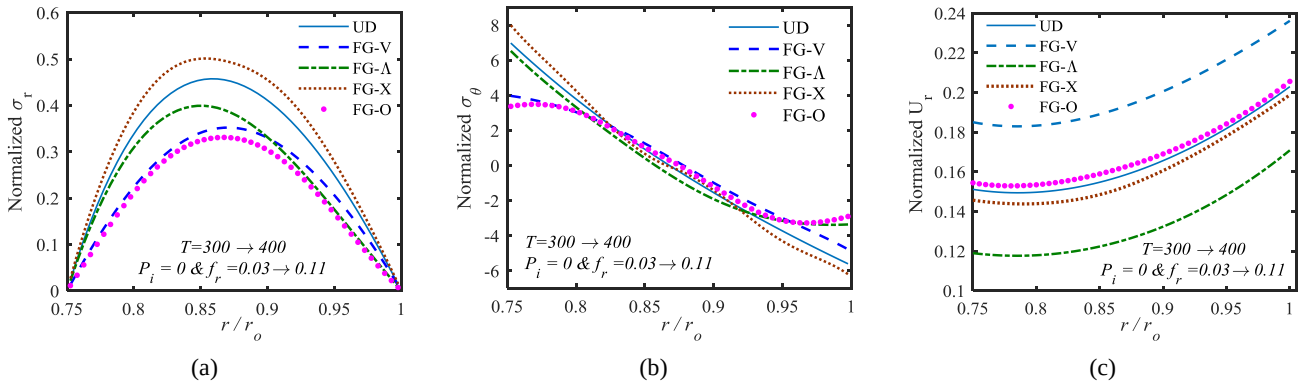

Fig. 5 Normalized (a) hoop stress; (b) radial stress; (c) radial deflection along the radius of thick cylinders under thermal gradient loads for different graphene distributions

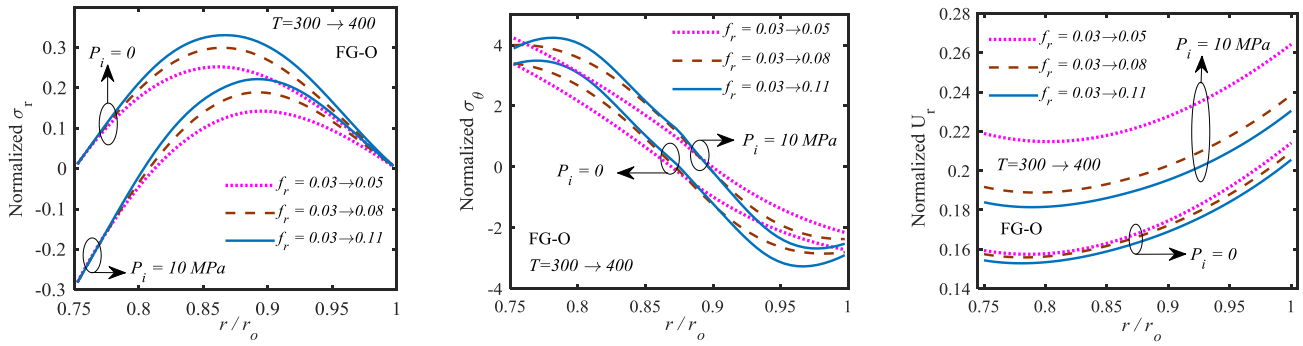

Fig. 6 Normalized (a) hoop stress; (b) radial stress; (c) radial deflection along the radius of O-GRNC thick cylinders under thermal gradient and mechanical loads for different graphene volume fractions

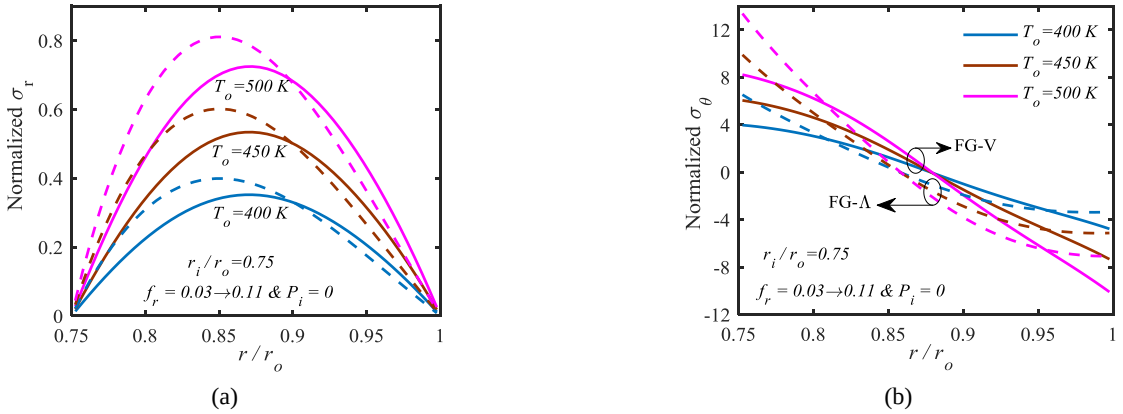

Fig. 7 Normalized (a) hoop stress; (b) radial stress along the radius of V and /\-GRNC thick cylinders with T_i = 300 K and r_i/r_o = 0.75 under different thermal gradient loads

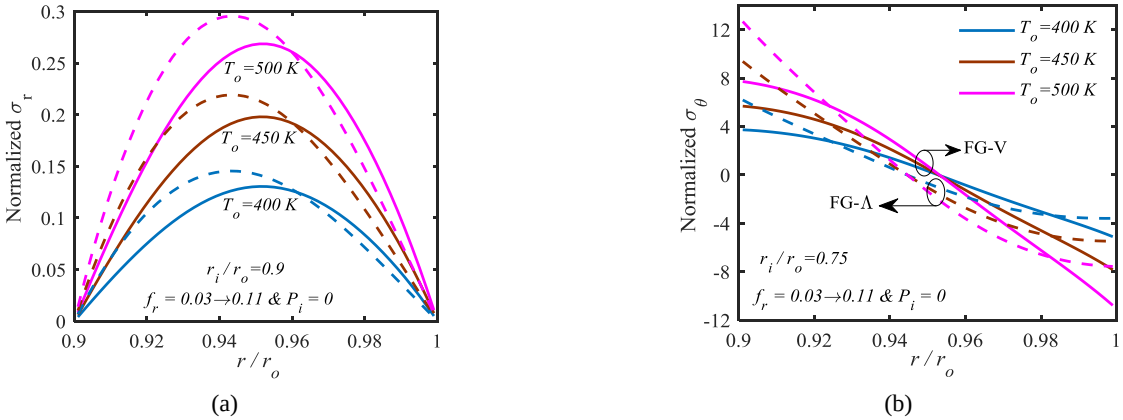

Fig. 8 Normalized (a) hoop stress; (b) radial stress along the radius of V and /\-GRNC thick cylinders with T_i = 300 K and r_i/r_o = 0.9 under different thermal gradient loads

0.9. It can be seen that rising thermal gradient load results in the increase of the values of stresses as well as the gradient of stresses along the thickness of GRNC cylinders. The maximum values of hoop stress are observed at the inner radius of /\-GRNC cylinders, however, it also happens at outer radius of V-GRNC cylinders. Comparison of Figs. 7 and 8 reveals that the decrease of cylinder thickness leads to a considerable decreasing in radial stresses, but it has an insignificant effect on hoop stress values. These results are in line with the exact results shown in Figs. 2(a) and (b).

4.3 Natural frequency of FG-GRNC cylinder

In this section, free vibration analysis of FG and UD-GRNC cylinder under thermal gradient effects are presented. Table 2 provides the first axisymmetric natural frequency parameters of clamped-clamped (C-C: U_r and U_z at two ends are fixed) and clamped-free (C-F) GRNC

Table 2 First frequency parameters of GRNC cylinders with r_i/r_o = 0.75, L/r_o = 1, f_r^{min} = 0.03 and f_r^{max} = 0.11

T (K)	C-C					C-F				
	UD	**Λ**	**X**	**V**	**O**	**UD**	**Λ**	**X**	**V**	**O**
300	14.5138	13.5956	13.9091	13.9573	13.5630	9.8096	9.2994	9.4709	9.4797	9.3651
350	14.0582	13.1452	13.4472	13.4931	13.1127	9.5017	8.9907	9.1562	9.1647	9.0542
400	13.7523	12.8682	13.1635	13.2080	12.8342	9.2949	8.7996	8.9616	8.9695	8.8613
500	13.4781	12.7093	13.0030	13.0468	12.6695	9.1096	8.6861	8.8467	8.8531	8.7455
300→400	14.0899	13.1240	13.5423	13.5443	13.1332	9.5169	8.9597	9.2241	9.1948	9.0609
400→300	14.0834	13.2366	13.4240	13.5218	13.1446	9.5232	9.0675	9.1330	9.1921	9.0774
300→500	13.8496	12.9149	13.3507	13.3528	12.9137	9.3500	8.8101	9.0867	9.0644	8.9001
500→300	13.8410	13.0526	13.2140	13.3269	12.9272	9.3583	8.9384	8.9826	9.0622	8.9195

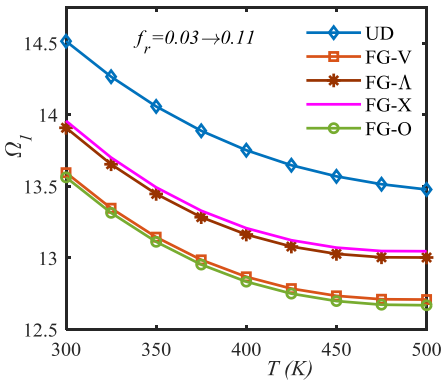

Fig. 9 First frequency parameters as a function of entire temperature of clamped-clamped GRNC cylinders with r_i/r_o = 0.75 and L/r_o = 1

cylinders with r_i/r_o = 0.75, L/r_o = 1, f_r^{min} = 0.03 and f_r^{max} = 0.11 for different thermal gradient loads and graphene profile distributions.

In C-C cylinders, UD and FG-O types have the highest and lowest values of natural frequencies, respectively. However, in the most cases of C-F cylinders, UD and FG-V types have those highest and lowest values, respectively. Due to having more constrains, the frequencies of C-C cylinders are much higher than C-F cylinders. By decreasing the elastic modulus of GRNC components and the stiffness of nanocomposite cylinders, rising the entire temperature of the cylinders or the improvement of thermal gradient loads results in a decrease in the natural frequency of nanocomposite cylinders. In UD-GRNC cylinders, the natural frequencies of cylinders under thermal gradient from inside to outside are higher than those under reverse thermal gradient. However, the natural frequencies of FG cylinders depend on both graphene distribution and thermal gradient direction.

Fig. 9 shows the first frequency parameters of clamped-clamped FG-GRNC cylinders with r_i/r_o = 0.75, L/r_o = 1, f_r^{min} = 0.03 and f_r^{max} = 0.11 as a function of the entire (environment) temperature of cylinders. Due to the smooth decrease of the mechanical stiffness of GRNC cylinders, the increase of temperature leads to smooth decreases in frequency parameters. Also, the significant effect of graphene distribution is clearly observed such that UD and FG-O cylinders have the highest and lowest values of frequencies for all considered temperatures.

The effects of graphene volume fraction and geometrical dimension are illustrated in Fig. 10 for clamped-clamped X-GRNC cylinders with T_i = 300 K and T_o = 400 K. Sharp increases in the frequencies of cylinders are observed by increasing the amount of graphene from f_r = 0.03 to 0.06, but further increase of graphene content from f_r = 0.08 to 0.1 has an insignificant effect. Moreover, the decrease of

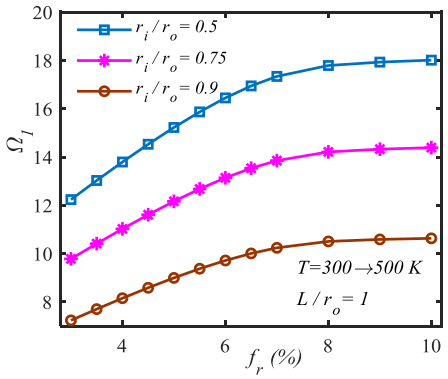

(a)

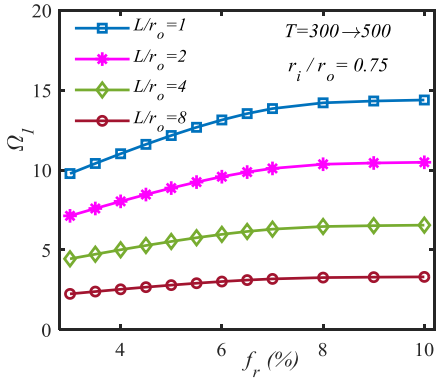

(b)

Fig. 10 First frequency parameters as a function of graphene volume fractions in clamped-clamped X-GRNC cylinders with T_i=300 K, T_o=400 K and (a) L/r_o = 1; (b) r_i/r_o = 0.75

thickness and/or increase of length caused considerable reductions in the natural frequencies of GRNC cylinders.

5. Conclusions

This paper developed an axisymmetric mesh-free method to study heat transfer, static response and natural frequency of thick cylinders reinforced with UD and FG randomly oriented graphene nano-sheets subjected to thermo-mechanical boundary conditions. A modified Halpin-Tsai model incorporated with efficiency parameters were employed to estimate the material properties of GRNC. The overall thermoelastic behavior of FG-GRNC cylinders were investigated and the following outcomes were found from our simulations:

- Depending on the surface temperatures, /\ and V-GRNC cylinders could have higher temperature than other profile types of graphene distributions.
- X-GRNC and O-GRNC cylinders under thermal gradient loads have the highest and lowest values of stresses, respectively.
- Increasing graphene volume fraction considerably increases the values of stresses in GRNC cylinders although reduces radial deflection.
- Rising thermal gradient load increases stress values and changes their locations along the thickness of FG-GRNC cylinders.
- In comparison with the distribution of graphene, its volume fraction has stronger effect on the natural frequencies of FG-GRNC cylinders.

Acknowledgments

The work described in this paper was supported by Natural Sciences and Engineering Research Council of Canada (NSERC under grant RGPIN-217525). The authors are grateful for their support.

References

Al-Mashat, L., Shin, K., Kalantar-zadeh, K., Plessis, J.D., Han, S.H., Kojima, R.W., Kaner, R.B., Li, D., Gou, X., Ippolito, S.J. and Wlodarski, W., (2010), "Graphene/polyaniline nanocomposite for hydrogen sensing", *The J. Phys. Chem. C*, **114**, 16168-16173.

Alian, A.R., Dewapriya, M.A.N. and Meguid, S.A. (2017), "Molecular dynamics study of the reinforcement effect of graphene in multilayered polymer nanocomposites", *Mater. Des.*, **124**, 47-57.

Alibeigloo, A. and Liew, K.M. (2013), "Thermoelastic analysis of functionally graded carbon nanotube-reinforced composite plate using theory of elasticity", *Compos. Struct.*, **106**, 873-881.

Arani, A.G., Zarei, M.S., Mohammadimehr, M., Arefmanesh, A. and Mozdianfard, M.R. (2011), "The thermal effect on buckling analysis of a DWCNT embedded on the Pasternak foundation", *Phys. E, Low-dimensional Syst. Nanostruct.*, **43**(9), 1642-1648.

Arani, A.G., Kolahchi, R., Barzoki, A.A.M., Mozdianfard, M.R. and Farahani, S.M.N. (2013), "Elastic foundation effect on nonlinear thermo-vibration of embedded double-layered orthotropic graphene sheets using differential quadrature method", *Proceed. Inst. Mech. Eng., Part C: J. Mech. Eng. Sci.*, **227**(4), 862-879.

Balandin, A.A., Ghosh, S., Bao, W., Calizo, I., Teweldebrhan, D., Miao, F. and Lau, C.N. (2008), "Superior thermal conductivity of single-layer graphene", *Nano Letters*, **8**(3), 902-907.

Craft, W.J. and Christensen, R.M. (1981), "Coefficient of thermal expansion for composites with randomly oriented fibers", *J. Compos. Mater.*, **15**(1), 2-20.

Cui, Y., Kundalwal, S.I. and Kumar, S. (2016), "Gas barrier performance of graphene/polymer nanocomposites", *Carbon*, **98**, 313-333.

Damadam, M., Moheimani, R. and Dalir, H. (2018), "Bree's diagram of a functionally graded thick-walled cylinder under thermo-mechanical loading considering nonlinear kinematic hardening", *Case Studies in Thermal Eng.*, **12**, 644-654.

Ebrahimi, F. and Barati, M.R. (2018), "A nonlocal strain gradient refined plate model for thermal vibration analysis of embedded graphene sheets via DQM", *Struct. Eng. Mech., Int. J.*, **66**(6), 693-701. http://dx.doi.org/10.12989/sem.2018.66.6.693

Fan, Y., Xiang, Y., Shen, H.S. and Hui, D. (2018), "Nonlinear low-velocity impact response of FG-GRC laminated plates resting on visco-elastic foundations", *Compos. Part B: Eng.*, **144**, 184-194.

Fan, Y., Xiang, Y. and Shen, H-S. (2019), "Nonlinear forced vibration of FG-GRC laminated plates resting on visco-Pasternak foundations", *Compos. Struct.*, **209**, 443-452.

Farahani, R.D., Pahlavanpour, M., Dalir, H., Aissa, B., El Khakani, M.A., Lévesque, M. and Therriault, D. (2012), "Manufacturing composite beams reinforced with three-dimensionally patterned-oriented carbon nanotubes through microfluidic infiltration", *Mater. Des.*, **41**, 214-225.

Gholami, R. and Ansari, R. (2018a), "Nonlinear harmonically excited vibration of third-order shear deformable functionally graded graphene platelet-reinforced composite rectangular plates", *Eng. Struct.*, **156**, 197-209.

Gholami, R. and Ansari, R. (2018b), "On the Nonlinear Vibrations of Polymer Nanocomposite Rectangular Plates Reinforced by Graphene Nanoplatelets: A Unified Higher-Order Shear Deformable Model", *Iran. J. Sci. Technol., Trans. Mech. Eng.* http://link.springer.com/10.1007/s40997-018-0182-9

Halpin, J.C. and Kardos, J.L. (1976), "The Halpin-Tsai equations: a review", *Polym. Eng. Sci.*, **16**, 344-352.

Hetnarski, R.B. and Eslami, M.R. (2009), *Thermal stresses-advanced theory and applications*, Springer, The Netherlands.

Hosseini, S.M. and Zhang, C. (2018), "Elastodynamic and wave propagation analysis in a FG graphene platelets-reinforced nanocomposite cylinder using a modified nonlinear micromechanical model", *Steel Compos. Struct., Int. J.*, **27**(3), 255-271. http://dx.doi.org/10.12989/scs.2018.27.3.255

Kiani, Y. and Mirzaei, M. (2018), "Enhancement of non-linear thermal stability of temperature dependent laminated beams with graphene reinforcements", *Compos. Struct.*, **186**, 114-122.

Konatham, D. and Striolo, A. (2009), "Thermal boundary resistance at the graphene-oil interface", *Appl. Phys. Lett.*, **95**, 163105.

Kumar, D. and Srivastava, A. (2016), "Elastic properties of CNT- and graphene-reinforced nanocomposites using RVE", *Steel Compos. Struct., Int. J.*, **21**(5), 1085-1103. http://dx.doi.org/10.12989/scs.2016.21.5.1085

Laoufi, I., Ameur, M., Zidi, M., Bedia, E.A.A. and Bousahla, A.A. (2016), "Mechanical and hygrothermal behaviour of functionally graded plates using a hyperbolic shear deformation theory", *Steel Compos. Struct., Int. J.*, **20**(4), 889-911.

Lei, Z., Su, Q., Zeng, H., Zhang, Y. and Yu, C. (2018), "Parametric studies on buckling behavior of functionally graded graphene-reinforced composites laminated plates in thermal

environment", *Compos. Struct.*, **202**, 695-709.
Li, M., Zhou, H., Zhang, Y., Liao, Y. and Zhou, H. (2018), "Effect of defects on thermal conductivity of graphene/epoxy nanocomposites", *Carbon*, **130**, 295-303.
Lin, F., Xiang, Y. and Shen, H.S. (2017), "Temperature dependent mechanical properties of graphene reinforced polymer nanocomposites - A molecular dynamics simulation", *Compos. Part B*, **111**, 261-269.
Malekzadeh, P., Setoodeh, A.R. and Shojaee, M. (2018), "Vibration of FG-GPLs eccentric annular plates embedded in piezoelectric layers using a transformed differential quadrature method", *Comput. Meth. Appl. Mech. Eng.*, **340**, 451-479.
Moheimani, R. and Ahmadian, M.T. (2012), "On Free Vibration of Functionally Graded Euler-Bernoulli Beam Models Based on the Non-Local Theory", In: *ASME International Mechanical Engineering Congress and Exposition, Volume 12: Vibration, Acoustics and Wave Propagation*, pp. 169-173.
Moheimani, R., Damadam, M., Nayebi, A. and Dalir, H. (2018), "Thick-walled functionally graded material cylinder under thermo-mechanical loading", In: *9th International Conference on Mechanical and Aerospace Engineering* (*ICMAE*) *IEEE*, pp. 505-510.
Moradi-Dastjerdi, R. and Payganeh, G. (2017a), "Thermoelastic dynamic analysis of wavy carbon nanotube reinforced cylinders under thermal loads", *Steel Compos. Struct., Int. J.*, **25**(3), 315-326. http://dx.doi.org/10.12989/scs.2017.25.3.315
Moradi-Dastjerdi, R. and Payganeh, G. (2017b), "Transient heat transfer analysis of functionally graded CNT reinforced cylinders with various boundary conditions", *Steel Compos. Struct., Int. J.*, **24**(3), 359-367. http://dx.doi.org/10.12989/scs.2017.24.3.359
Moradi-Dastjerdi, R. and Payganeh, G. (2018), "Thermoelastic vibration analysis of functionally graded wavy carbon nanotube-reinforced cylinders", *Poly. Compos.*, **39**(S2), E826-E834.
Moradi-Dastjerdi, R. and Pourasghar, A. (2016), "Dynamic analysis of functionally graded nanocomposite cylinders reinforced by wavy carbon nanotube under an impact load", *J. Vib. Control*, **22**, 1062-1075.
Moradi-Dastjerdi, R., Payganeh, G. and Tajdari, M. (2017), "Resonance in Functionally Graded Nanocomposite Cylinders Reinforced by Wavy Carbon Nanotube", *Poly. Compos.*, **38**, E542-E552.
Moradi-Dastjerdi, R., Payganeh, G. and Tajdari, M. (2018), "Thermoelastic Analysis of Functionally Graded Cylinders Reinforced by Wavy CNT Using a Mesh-Free Method", *Poly. Compos.*, **39**(7), 2190-2201.
Novoselov, K.S., Geim, A.K., Morozov, S.V., Jiang, D., Zhang, Y., Dubonos, S.V., Grigorieva, I.V. and Firsov, A.A. (2004), "Electric field effect in atomically thin carbon films", *Sci.*, **306**(5696), 666-669.
Pourasghar, A. and Chen, Z. (2016), "Thermoelastic response of CNT reinforced cylindrical panel resting on elastic foundation using theory of elasticity", *Compos. Part B*, **99**(15), 436-444.
Pourasghar, A., Moradi-Dastjerdi, R., Yas, M.H., Ghorbanpour Arani, A. and Kamarian, S. (2018), "Three-dimensional analysis of carbon nanotube-reinforced cylindrical shells with temperature-dependent properties under thermal environment", *Poly. Compos.*, **39**(4), 1161-1171.
Rafiee, M.A., Rafiee, J., Yu, Z.Z. and Koratkar, N. (2009), "Buckling resistant graphene nanocomposites", *Appl. Phys. Letters*, **95**(22), 223103.
Safaei, B. and Fattahi, A.M. (2017), "Free vibrational response of single-layered graphene sheets embedded in an elastic matrix using different nonlocal plate models", *MECHANIKA*, **23**(5), 678-687.
Safaei, B., Moradi-Dastjerdi, R. and Chu, F. (2018), "Effect of thermal gradient load on thermo-elastic vibrational behavior of sandwich plates reinforced by carbon nanotube agglomerations", *Compos. Struct.*, **192**, 28-37.
Safaei, B., Moradi-Dastjerdi, R., Qin, Z. and Chu, F. (2019), "Frequency-dependent forced vibration analysis of nanocomposite sandwich plate under thermo-mechanical loads", *Compos. Part B*, **161**, 44-54.
Safari, S., Moradi-Dastjerdi, R., Nezam Abadi, A. and Tajdari, M. (2018), "Vibration behavior of magnetorheological-filled functionally graded nanocomposite cylinders reinforced by carbon nanotube", *Poly. Compos.*, **39**(S2), E1005-E1012.
Setoodeh, A.R. and Badjian, H. (2017), "Mechanical behavior enhancement of defective graphene sheet employing boron nitride coating via atomistic study", *Mater. Res. Express*, **4**(12), 125019.
Shen, X., Wang, Z., Wu, Y., Liu, X., He, Y.B. and Kim, J.K. (2016), "Multilayer graphene enables higher efficiency in improving thermal conductivities of graphene/epoxy composites", *Nano Letters* **16**(6), 3585-3593.
Shen, H.S., Lin, F. and Xiang, Y. (2017a), "Nonlinear bending and thermal postbuckling of functionally graded graphene-reinforced composite laminated beams resting on elastic foundations", *Eng. Struct.*, **140**, 89-97.
Shen, H.S., Xiang, Y. and Lin, F. (2017b), "Nonlinear bending of functionally graded graphene-reinforced composite laminated plates resting on elastic foundations in thermal environments", *Compos. Struct.*, **170**, 80-90.
Shen, H.S., Xiang, Y., Fan, Y. and Hui, D. (2018), "Nonlinear bending analysis of FG-GRC laminated cylindrical panels on elastic foundations in thermal environments", *Compos. Part B*, **141**, 148-157.
Sobhaniaragh, B., Batra, R.C., Mansur, W.J. and Peters, F.C. (2017), "Thermal response of ceramic matrix nanocomposite cylindrical shells using Eshelby-Mori-Tanaka homogenization scheme", *Compos. Part B*, **118**, 41-53.
Song, M., Kitipornchai, S. and Yang, J. (2017), "Free and forced vibrations of functionally graded polymer composite plates reinforced with graphene nanoplatelets", *Compos. Struct.*, **159**, 579-588.
Song, M., Yang, J. and Kitipornchai, S. (2018), "Bending and buckling analyses of functionally graded polymer composite plates reinforced with graphene nanoplatelets", *Compos. Part B*, **134**, 106-113.
Sun, Y. and Shi, G. (2013), "Graphene/polymer composites for energy applications", *J. Poly. Sci., Part B: Poly. Phys.*, **51**(4), 231-253.
Wu, H., Yang, J. and Kitipornchai, S. (2018), "Parametric instability of thermo-mechanically loaded functionally graded graphene reinforced nanocomposite plates", *Int. J. Mech. Sci.*, **135**, 431-440.
Yang, Y.H., Bolling, L., Priolo, M.A. and Grunlan, J.C. (2013), "Super gas barrier and selectivity of graphene oxide-polymer multilayer thin films", *Adv. Mater.*, **25**(4), 503-508.
Yang, B., Kitipornchai, S., Yang, Y.F. and Yang, J. (2017), "3D thermo-mechanical bending solution of functionally graded graphene reinforced circular and annular plates", *Appl. Math. Modelling*, **49**, 69-86.
Yang, B., Mei, J., Chen, D., Yu, F. and Yang, J. (2018), "3D thermo-mechanical solution of transversely isotropic and functionally graded graphene reinforced elliptical plates", *Compos. Struct.*, **184**, 1040-1048.
Yu, Y., Shen, H.S., Wang, H. and Hui, D. (2018), "Postbuckling of sandwich plates with graphene-reinforced composite face sheets in thermal environments", *Compos. Part B*, **135**, 72-83.

Appendix

The exact solutions of temperature and stress distributions in isotropic thick cylinders subjected to thermal gradient loads reported by Hetnarski and Eslami (2009) are

$$T = \frac{T_i - T_o}{\ln(r_o / r_i)} \ln(r_o / r) + T_o \tag{A1}$$

$$\sigma_r = \frac{E\alpha(T_i - T_o)}{2(1-\upsilon)\ln(r_o / r_i)} \times \left[\ln(r_o / r) + \frac{r_i^2}{r_o^2 - r_i^2}\left(1 - \frac{r_o^2}{r^2}\right)\ln(r_o / r_i) \right] \tag{A2}$$

$$\sigma_\theta = \frac{E\alpha(T_i - T_o)}{2(1-\upsilon)\ln(r_o / r_i)} \times \left[1 - \ln(r_o / r) - \frac{r_i^2}{r_o^2 - r_i^2}\left(1 + \frac{r_o^2}{r^2}\right)\ln(r_o / r_i) \right] \tag{A3}$$